A METHOD OF DETERMINING GEOMETRY OF CONE BEAM CT SCANNER

O TISCHENKO[1], N SAEID NEZHAD[2] AND C HOESCHEN[2]

Abstract. The task of determining the geometry of a cone-beam CT scanner with flat panel detector and circular/spiral source trajectory is considered. Accomplishing this task implies analyzing projections of a set of points referred to as calibrating set or calibrating phantom. We take advantage of the fact that observed coordinates of a point's projection are rational functions of the point's location. Unknown coefficients of these functions can be recovered exactly from six projections of the point. Location of the source as well as position and orientation of the detector are determined in the scanner reference frame, which is constituted by rotation axis and central plane of the scanner. Two different projections of a calibrating set are enough to solve the task if the source trajectory is a circle. In applications where a shift of an object transversally to the central plane is required, two additional projections have to be collected in order to identify the direction of the shift. The developed formalism becomes especially simple when the detector is aligned with the rotation axis. In this case four projections of a single calibrating point rotated successfully about the rotation axis are sufficient. The error analysis carried out in the paper shows that the magnitude of deviation from the true values is of the order of the magnitude of measurement errors.

1. Introduction

In the computer tomography data are collected in form of integrals of a quantity of interest, e.g. the attenuation coefficient, measured over rays crossing an investigated object. In the practice, correct associating the collected data with rays is crucial for the quality of the reconstruction and is possible only if a scanner's geometry is known. As scanner's geometry one refers to a set of system parameters describing a spatial configuration of the scanner's essential components which are a source focus, a detector and a rotation stage designed for rotating an object under study.

Relative to the rotation stage a cone beam CT scanner, regarded as a mechanical system, has nine degrees of freedom, three for the source location, three for the detector position, and three for the angular orientation of the detector. For a scanner with circular source trajectory and constant distance between the source and the detector the number of degrees of freedom is reduced by two. Accordingly, there are seven kinematically independent system parameters which have to be estimated.

Depending on the type of the scanner a process of estimating the system parameters, referred usually to as geometric calibration, has to be carried out every time before the investigation of the patient, or once over certain period of time.

Date: July 16, 2019.

Various methods allowing one to determine the scanner geometry have been proposed in the literature. Depending on certain criteria they may undergo different classifications. In terms of the background formalism used for the calibration they can be classified as analytic ([2], [4], [6], [12], [13], [18], [19], [21]) and optimization ([1], [3], [5], [7]-[10], [15], [17], [22]) methods. The methods based on pre-scans of a marker phantom are classified as offline methods. These methods assume that the geometry of the CT scanner is the same both during calibration and in subsequent scans, which is a reasonable assumption for many systems. A problem with the methods using a marker phantom is that the phantom being normally designed for a particular acquisition trajectory is not applicable to a diversity of trajectories. So-called online methods generally address cases in which the acquisition trajectory is not reproducible, e.g. due to so-called flex of the rotation axis or patient motion. These methods allow one to estimate geometry directly from the patient scan. Some of them employ the data redundancy conditions [15], [16]. In [11], [20] anticipated properties in the reconstruction via iterative optimization are enforced, while the method proposed in [3] is based on the formalism of the consistency conditions for linear integral operator. Common to these methods is that they make use of iterative optimization algorithms which are expensive in terms of computational complexity.

CT cone beam scanners as well as pinhole SPECT scanners with circular/spiral source trajectory constituting an important class of scanners can be calibrated with the methods mentioned above. However, some of them give a restricted solution of the problem or require using a phantom that is challenging to manufacture. In [13] a method is proposed that can be used under condition that the detector is aligned with the rotation axis. This method requires a set of projections of a simple phantom consisting of two points rotated successively around the rotation axis. Similar phantom, but consisting of a single point, is used in [19]. There, under assumption that the components of a circle projection are trigonometric polynomials of degree ≥ 3, an orientation of the detector and a position of the origin of the detector relative to the source are determined. However both the source to rotation axis and the source to detector distances remain undetermined. In [21] a more complicated phantom consisting of several points is used to determine geometry of the scanner the detector of which is aligned with the rotation axis and the line connecting the source and the iso-center is perpendicular to the detector plane. In [4], using a complex calibrating phantom, one determines six system parameters, while the source to rotation axis distance is obtained in the sense of homogeneous coordinates. In the method proposed in [1] the iterative Powell algorithm was used to estimate geometry of a pinhole SPECT scanner. Some *a priori* knowledge of the scanner geometry, that can be measured up to some reasonable accuracy, is necessary for this method to assure that the iterative process converges to a correct solution. The method proposed in [5] refines the estimates of the extrinsic parameters obtained in [1]. Both mentioned methods make use of iterative optimization starting from multipoint phantoms, with thorough analysis of the correlation between some misalignment parameters that may hamper the calibration task unless some constraint is applied. Using simple formalism with minimal requirements on phantom the method proposed in [12] can be applied for estimating a scanner's pose relative to the calibrating phantom. However the only intrinsic parameters determined in [12] are the focus to detector distance and the

orthogonal projection of the source onto the detector. But the source position as well as the detector orientation are given there in a so-called laboratory reference frame, the center of which is a point of the phantom, and the axes are the symmetry axes of the phantom. In other words the rays crossing the patient are assumed to be coordinated in the laboratory frame. Indeed, it might be useful to modify the method cited above in order to determine the focus to detector distance as well as the position and the orientation of the detector in the scanner reference frame.

In this paper we propose an analytic method of the calibration of a cone beam CT scanner with a circular/spiral acquisition trajectory. Though developed independently, the formalism laid in the background of the method is similar to that one used in [12]. In contrast in the proposed paper the values of all system parameters are given in the scanner reference frame. Two projections of a simple calibrating phantom have to be acquired to determine the scanner geometry completely. The developed in sections 3 and 4 formalism of the method can be directly applied to the case where the rotation axis is parallel to the detector plane. As was shown in sections 5, in this case only four projections of a single calibrating point are sufficient. Section 6 provides with error bounds for the most system parameters, and gives an idea of how the geometry of the calibrating setup may affect accuracy of the calibration. It was shown that the method is robust with respect to measurements errors and small deviations from presumably perfect phantom geometry and location of the phantom relative to scanner. Finally, performance of the method was evaluated for the accuracy of the parameter estimates. The results of the evaluation are presented in section 7.

2. Notations and Problem statement

CT scanner designed for collecting cone-beam projections is considered. The scanner is combined of x-ray source and flat panel detector, both fixed in space. Between the source and the detector there is a precision rotation stage provided for rotating the object under study. Schematic arrangement of the scanner is shown in figure 3. In this figure axis Oz is the rotation axis; Oxy is central plane, i.e. the plane that contains the source and is perpendicular to the rotation axis; l is line of the intersection of the central plane and the detector plane. Reference frame $Oxyz$ is referred in the following to as scanner reference frame. This frame, as well as all other reference frames introduced below, is assumed to be orthogonal. There are different choices to direct axes x and y. We direct them perpendicularly and parallel to line l respectively (see Fig. 3). The detector is supplied with its own reference frame to which we refer as observation reference frame. The axes of this frame, which we denote as u, v, are assumed to be parallel to the rows and columns of the matrix of the detector respectively. The orientation of the detector in the scanner reference frame can be described by two angles, angle β between the detector plane and the rotation axis, and angle γ between the u-axis of the observation reference frame and line l. Denote with $\mathcal{B}$ and $\mathcal{G}$ matrices of basic rotations

$$\mathcal{B} = \begin{pmatrix} \cos\beta & 0 & -\sin\beta \\ 0 & 1 & 0 \\ \sin\beta & 0 & \cos\beta \end{pmatrix}, \quad \mathcal{G} = \begin{pmatrix} 1 & 0 & 0 \\ 0 & \cos\gamma & \sin\gamma \\ 0 & -\sin\gamma & \cos\gamma \end{pmatrix}, \tag{1}$$

and let $O\xi\eta\zeta$ be the reference frame such that the components of a point in frames $Oxyz$ and $O\xi\eta\zeta$ relate to each other via transformation

$$\begin{pmatrix}\xi\\ \eta\\ \zeta\end{pmatrix} = \mathcal{GB}\begin{pmatrix}x\\ y\\ z\end{pmatrix}. \tag{2}$$

From the definitions of angles β and γ it follows that the ξ-axis is perpendicular to the detector plane, while axes η and ζ are parallel to axes u and v respectively. In the following we refer to $O\xi\eta\zeta$ as detector reference frame. For a point (u, v) of the detector plane, relation

$$\begin{pmatrix}\xi\\ \eta\\ \zeta\end{pmatrix} = \boldsymbol{R} + \begin{pmatrix}0\\ u\\ v\end{pmatrix} \tag{3}$$

is valid, where ξ, η, ζ are the components of the point in frame $O\xi\eta\zeta$, and vector $\boldsymbol{R}$ points from origin O to the reference point of the detector, which may be chosen arbitrarily. Finally, the location of the source focus is denoted as $\boldsymbol{F}$. Due to the definition, according to which $\boldsymbol{F} \in Oxy$, in the scanner reference frame $\boldsymbol{F} = (F_x, F_y, 0)$.

For a point $\boldsymbol{p} \neq \boldsymbol{F}$ there is a ray starting in source $\boldsymbol{F}$ and passing through this point. The point in which the ray intersects the detector plane is referred to as x-ray projection of $\boldsymbol{p}$. Denote with D the source to detector distance, and with $\boldsymbol{\mathcal{P}}$ the orthogonal projection of $\boldsymbol{F}$ onto the detector plane. Then

$$D = F_\xi - R_\xi, \quad \mathcal{P}_u = F_\eta - R_\eta, \quad \mathcal{P}_v = F_\zeta - R_\zeta, \tag{4}$$

where $\mathcal{P}_u, \mathcal{P}_v$ are the components of $\boldsymbol{\mathcal{P}}$ in the observation reference frame, and $F_i, R_i, i \in \{\xi, \eta, \zeta\}$, are the components of vectors $\boldsymbol{F}, \boldsymbol{R}$ in reference frame $O\xi\eta\zeta$. The x-ray projection of point $\boldsymbol{p} = (\xi, \eta, \zeta)$ is given by equation

$$\begin{pmatrix}0\\ u\\ v\end{pmatrix} = \begin{pmatrix}D\\ \mathcal{P}_u\\ \mathcal{P}_v\end{pmatrix} + \begin{pmatrix}\xi - F_\xi\\ \eta - F_\eta\\ \zeta - F_\zeta\end{pmatrix}\tau(\boldsymbol{p}), \tag{5}$$

where

$$\tau(\boldsymbol{p}) = \frac{D}{F_\xi - \xi} > 1. \tag{6}$$

The parameters of set

$$\Omega := \{\beta, \gamma, F_x, F_y, D, \mathcal{P}_u, \mathcal{P}_v\} \tag{7}$$

completely describe the geometry of the scanner in the scanner reference frame, that is, any other system parameter can be expressed through parameters of set Ω. In particular components of vector $\boldsymbol{R}$ can be expressed through parameters of Ω with the help of (4). Three more parameters must be determined if a shift of the object under study transversally to the central plane is provided. These are the components of vector $\boldsymbol{e}$ directed along the shift.

Determining the parameters of set Ω implies measuring projections of a set of calibrating points such that

(1) projections of the points of the set can be observed in the observation reference frame,
(2) for any two points $\boldsymbol{p}_1, \boldsymbol{p}_2$ of the set the components of vector $\Delta\boldsymbol{p} = \boldsymbol{p}_2 - \boldsymbol{p}_1$ are known in some well defined reference frame.

In other words the notion of a calibrating set implies existence of the reference frame that can be used for the description of the mutual arrangement of the calibrating points. We refer to this frame as calibrating reference frame.

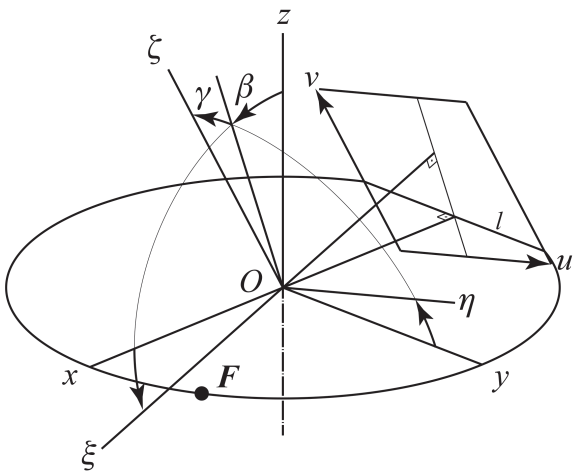

FIGURE 1. Arrangement of the scanner. $Oxyz$ is the scanner reference frame; Oz is the rotation axis, and Oxy is the central plane of the scanner. Line l is the line of the intersection of the central plane and the detector plane coordinated with u, v; axes Ox and Oy are perpendicular and parallel to line l respectively. Axis $O\xi$ is normal to the detector plane; $O\eta$ is parallel to u-axis of the detector, and $O\zeta$ is parallel to v-axis; $\boldsymbol{F}$ is the focus of the source.

3. Determining unknown parameters

Let $\boldsymbol{p}_0$ be some fixed point, and let $Ot^0s^0h^0$ be a reference frame in which the components $\Delta t, \Delta s, \Delta h$ of vector $\Delta\boldsymbol{p} = \boldsymbol{p} - \boldsymbol{p}_0$ are known for any point $\boldsymbol{p}$. In the following this frame is called calibrating reference frame; point $\boldsymbol{p}_0$ is called initial point. Representation

$$\begin{pmatrix}\xi\\ \eta\\ \zeta\end{pmatrix} = \begin{pmatrix}\xi_0\\ \eta_0\\ \zeta_0\end{pmatrix} + \Theta^0 \begin{pmatrix}\Delta t\\ \Delta s\\ \Delta h\end{pmatrix}, \tag{8}$$

is valid, where (ξ_0, η_0, ζ_0) and (ξ, η, ζ) are the components of $\boldsymbol{p}_0$ and $\boldsymbol{p}$ in $O\xi\eta\zeta$, and

$$\Theta^0 = \mathcal{G}\mathcal{B}\mathcal{A}^0 = \begin{pmatrix}\theta^0_{\xi,t} & \theta^0_{\xi,s} & \theta^0_{\xi,h}\\ \theta^0_{\eta,t} & \theta^0_{\eta,s} & \theta^0_{\eta,h}\\ \theta^0_{\zeta,t} & \theta^0_{\zeta,s} & \theta^0_{\zeta,h}\end{pmatrix} \tag{9}$$

is a matrix of transformation from $Ot^0s^0h^0$ to $O\xi\eta\zeta$; matrix

$$\mathcal{A}^0 = \begin{pmatrix}\alpha_{x,t} & \alpha_{x,s} & \alpha_{x,h}\\ \alpha_{y,t} & \alpha_{y,s} & \alpha_{y,h}\\ \alpha_{z,t} & \alpha_{z,s} & \alpha_{z,h}\end{pmatrix} \tag{10}$$

is a matrix of transformation from $Ot^0s^0h^0$ to $Oxyz$; matrices $\mathcal{B}$ and $\mathcal{G}$ are defined in (1). Let $\boldsymbol{\theta}^0_\xi, \boldsymbol{\theta}^0_\eta, \boldsymbol{\theta}^0_\zeta$ denote the rows of matrix Θ^0. After substitution of (8) into

(5) it becomes possible to represent the observed components of the projection of $\boldsymbol{p}$ in form

$$u = \frac{u_0 + \langle \boldsymbol{a}^0, \Delta\boldsymbol{p}\rangle}{1 + \langle \boldsymbol{c}^0, \Delta\boldsymbol{p}\rangle}, \quad v = \frac{v_0 + \langle \boldsymbol{b}^0, \Delta\boldsymbol{p}\rangle}{1 + \langle \boldsymbol{c}^0, \Delta\boldsymbol{p}\rangle}. \tag{11}$$

Here $\langle\cdot,\cdot\rangle$ is the dot product of 3-vectors; u_0, v_0 are the observed components of the projection of $\boldsymbol{p}_0$; unknown vectors $\boldsymbol{a}^0, \boldsymbol{b}^0, \boldsymbol{c}^0$ are represented by

$$\boldsymbol{c}^0 = -\frac{\tau_0}{D}\boldsymbol{\theta}^0_\xi, \quad \boldsymbol{a}^0 = \tau_0\boldsymbol{\theta}^0_\eta + \mathcal{P}_u\boldsymbol{c}^0, \quad \boldsymbol{b}^0 = \tau_0\boldsymbol{\theta}^0_\zeta + \mathcal{P}_v\boldsymbol{c}^0, \tag{12}$$

with

$$\tau_0 = \tau(\boldsymbol{p}_0) = D/(F_\xi - \xi_0). \tag{13}$$

As one can see in (11), the projections of a point $\boldsymbol{p}$ are expressed as rational functions of known variables $\Delta t, \Delta s, \Delta h$. Unknown coefficients $\boldsymbol{a}^0, \boldsymbol{b}^0$ and $\boldsymbol{c}^0$ of these functions can be determined from few samples of these functions uniquely. A set of the sampling points allowing to accomplish this is referred to in the following as calibrating set, or calibrating phantom. In section 4 we consider a simple calibrating set consisting of six points located in the vertices of the octahedron. So far the vectors $\boldsymbol{a}^0, \boldsymbol{b}^0, \boldsymbol{c}^0$ are assumed to be known.

Using orthogonality of matrix Θ^0, one finds that

$$D = \frac{\|\boldsymbol{a}^0 \times \boldsymbol{c}^0\|}{\|\boldsymbol{c}^0\|^2} = \frac{\|\boldsymbol{b}^0 \times \boldsymbol{c}^0\|}{\|\boldsymbol{c}^0\|^2} \tag{14}$$

$$\mathcal{P}_u = \frac{\langle \boldsymbol{a}^0, \boldsymbol{c}^0\rangle}{\|\boldsymbol{c}^0\|^2}, \quad \mathcal{P}_v = \frac{\langle \boldsymbol{b}^0, \boldsymbol{c}^0\rangle}{\|\boldsymbol{c}^0\|^2} \tag{15}$$

where $\|\boldsymbol{c}\| = \sqrt{\langle \boldsymbol{c}, \boldsymbol{c}\rangle}$, and $\times$ means the cross product. Hence, the focus to detector distance D and the components $\mathcal{P}_u, \mathcal{P}_v$ of the orthogonal projection of the focus can be determined from one projection of the calibrating set.

For determining angles β, γ as well as location $\boldsymbol{F}$ of the source in the scanner reference system, one additional projection is necessary. Rotate the calibrating set about the rotation axis at angle π, and denote the rotated calibrating frame as $Ot^1s^1h^1$. Let Θ^1 be a matrix of transformation from $Ot^1s^1h^1$ to $O\xi\eta\zeta$. It is clear that

$$\Theta^1 = \mathcal{G}\mathcal{B}\mathcal{A}^1 = \begin{pmatrix} \theta^1_{\xi,t} & \theta^1_{\xi,s} & \theta^1_{\xi,h} \\ \theta^1_{\eta,t} & \theta^1_{\eta,s} & \theta^1_{\eta,h} \\ \theta^1_{\zeta,t} & \theta^1_{\zeta,s} & \theta^1_{\zeta,h} \end{pmatrix} \tag{16}$$

where

$$\mathcal{A}^1 = \begin{pmatrix} -\alpha_{x,t} & -\alpha_{x,s} & -\alpha_{x,h} \\ -\alpha_{y,t} & -\alpha_{y,s} & -\alpha_{y,h} \\ \alpha_{z,t} & \alpha_{z,s} & \alpha_{z,h} \end{pmatrix}, \tag{17}$$

with $\alpha_{i,j}$ defined in (10), is a matrix of transformation from $Ot^1s^1h^1$ to $Oxyz$. Denote the location, the initial point moves to after the rotation, as $\boldsymbol{p}_1$, and let $\tau_1 = \tau(\boldsymbol{p}_1)$. Denote with $\boldsymbol{a}^1, \boldsymbol{b}^1$ and $\boldsymbol{c}^1$ the vectors obtained by analogy with the vectors $\boldsymbol{a}^0, \boldsymbol{b}^0$ and $\boldsymbol{c}^0$ respectively. One can express the rows of matrices Θ^k, $k = 0, 1$, through vectors $\boldsymbol{a}^k, \boldsymbol{b}^k$ and $\boldsymbol{c}^k$, and find that for any $i \in \{t, s, h\}$

$$\theta^0_{\xi,i} + \theta^1_{\xi,i} = -2\alpha_{z,i}\sin\beta =: \omega_{\xi,i}, \tag{18}$$

$$\theta^0_{\eta,i} + \theta^1_{\eta,i} = 2\alpha_{z,i}\sin\gamma\cos\beta =: \omega_{\eta,i}/D, \tag{19}$$

$$\theta^0_{\zeta,i} + \theta^1_{\zeta,i} = 2\alpha_{z,i}\cos\gamma\cos\beta =: \omega_{\zeta,i}/D. \tag{20}$$

Therefore

$$\tan\gamma = \frac{\omega_{\eta,i}}{\omega_{\zeta,i}}, \tag{21}$$

and

$$\tan\beta = -\frac{\omega_{\xi,i}}{\omega_{\zeta,i}} D\cos\gamma. \tag{22}$$

Both (21) and (22) must hold for any i. However, for some i both of them may happen to be numerically unstable, e.g. if $\alpha_{z,i}$ is close to zero. Therefore the subscript reliable in terms of numerical stability of formulas (21) and (22) has to be chosen. This should always exist. In the following we assume that angles β, γ as well as the angle between axes z and h substantially differ from $\pm\pi/2$. Then term $\omega_{\zeta,h}$ substantially differs from zero, which guarantees numerical stability of the above formulas when $i = h$. Under this assumption

$$\tan\gamma = \frac{(a_h^0 - \mathcal{P}_u c_h^0)/\|\boldsymbol{c}^0\| + (a_h^1 - \mathcal{P}_u c_h^1)/\|\boldsymbol{c}^1\|}{(b_h^0 - \mathcal{P}_v c_h^0)/\|\boldsymbol{c}^0\| + (b_h^1 - \mathcal{P}_v c_h^1)/\|\boldsymbol{c}^1\|}, \tag{23}$$

and

$$\tan\beta = \frac{c_h^0/\|\boldsymbol{c}^0\| + c_h^1/\|\boldsymbol{c}^1\|}{(b_h^0 - \mathcal{P}_v c_h^0)/\|\boldsymbol{c}^0\| + (b_h^1 - \mathcal{P}_v c_h^1)/\|\boldsymbol{c}^1\|} D\cos\gamma. \tag{24}$$

In order to derive expressions for F_x and F_y one can set $\boldsymbol{p} = \boldsymbol{p}_0$ in (5) and rewrite it in the scanner reference frame $Oxyz$. One obtains

$$\begin{pmatrix} F_x - x_0 \\ F_y - y_0 \\ F_z - z_0 \end{pmatrix} = \frac{1}{\tau_0} (\mathcal{G}\mathcal{B})^T \begin{pmatrix} D \\ \mathcal{P}_u - u_0 \\ \mathcal{P}_v - v_0 \end{pmatrix}. \tag{25}$$

Similarly, setting $\boldsymbol{p} = \boldsymbol{p}_1$ in (5) and recalling that $\boldsymbol{p}_1 = (-x_0, -y_0, z_0)$, one can obtain equation

$$\begin{pmatrix} F_x + x_0 \\ F_y + y_0 \\ F_z - z_0 \end{pmatrix} = \frac{1}{\tau_1} (\mathcal{G}\mathcal{B})^T \begin{pmatrix} D \\ \mathcal{P}_u - u_1 \\ \mathcal{P}_v - v_1 \end{pmatrix}. \tag{26}$$

Accounting for condition $F_z = 0$ from (25) and (26) one derives representation

$$\begin{pmatrix} x_0 \\ y_0 \\ z_0 \end{pmatrix} = \frac{1}{2} \begin{pmatrix} \left(\tau_1^{-1} - \tau_0^{-1}\right) D\sec\beta \\ U_0/\tau_0 - U_1/\tau_1 \\ 2R_z/\tau_0 \end{pmatrix}. \tag{27}$$

and

$$\begin{pmatrix} F_x \\ F_y \end{pmatrix} = \begin{pmatrix} x_0 + \tau_0^{-1} R_x \\ -\frac{1}{2}(\tau_0^{-1} U_0 + \tau_1^{-1} U_1) \end{pmatrix} \tag{28}$$

where $R_z = V_0\cos\beta + D\sin\beta$, $R_x = -V_0\sin\beta + D\cos\beta$ and for $k = 0, 1$

$$\begin{pmatrix} U_k \\ V_k \end{pmatrix} = \begin{pmatrix} \cos\gamma & -\sin\gamma \\ \sin\gamma & \cos\gamma \end{pmatrix} \begin{pmatrix} u_k - \mathcal{P}_u \\ v_k - \mathcal{P}_v \end{pmatrix}. \tag{29}$$

Representation (27) can be used for identifying the direction of a shift of an object under study, e.g. a patient, transversally to the central plane in applications where such a shift is required. Indeed, the direction of the shift can be identified as the direction of the line connecting points $\boldsymbol{p}_0$ and $\boldsymbol{p}_{0,s}$, where $\boldsymbol{p}_{0,s}$ is the location of the initial point in the scanner reference frame after the shift.

4. Calibrating Set

As calibrating set we consider the vertices of the octahedron. This set is advantageous both in terms of its simple geometry and in terms of the simplicity of the expressions obtained for coefficients $\boldsymbol{a}, \boldsymbol{b}, \boldsymbol{c}$ when the points of the set are treated as sampling points of rational functions defined by (11). Also in the case when the detector is aligned with the rotation axis, as to be regarded in the next section, considering this set significantly simplifies solution of the problem.

Let the distance between the opposite vertices of the octahedron be 2Δ. Then there exists an orthogonal reference frame $Otsh$ in which

$$\boldsymbol{p}_{\pm t} - \boldsymbol{p}_0 = (\pm\Delta, 0, 0), \quad \boldsymbol{p}_{\pm s} - \boldsymbol{p}_0 = (0, \pm\Delta, 0), \quad \boldsymbol{p}_{\pm h} - \boldsymbol{p}_0 = (0, 0, \pm\Delta), \tag{30}$$

where $\boldsymbol{p}_{\pm t}, \boldsymbol{p}_{\pm s}, \boldsymbol{p}_{\pm h}$ and $\boldsymbol{p}_0$ are locations of the vertices and of the center of the octahedron respectively. Clearly, the projection of the center of the octahedron can be identified as the intersection of the lines connecting the projections of the opposite vertices. So in fact this calibrating set consists of six points.

Let $(u_{\pm i}, v_{\pm i})$ be observed components of the projection of calibrating point $\boldsymbol{p}_{\pm i}$, $i \in \{t, s, h\}$. Rewrite (11) in form

$$\langle \boldsymbol{a} - u\boldsymbol{c}, \Delta\boldsymbol{p} \rangle = u - u_0, \quad \langle \boldsymbol{b} - v\boldsymbol{c}, \Delta\boldsymbol{p} \rangle = v - v_0 \tag{31}$$

where for the sake of simplicity of notations superscript 0 of elements $\boldsymbol{a}, \boldsymbol{b}, \boldsymbol{c}$ has been omitted. Substituting (30) into the above equations yields two pairs of equations relative to unknowns a_i, c_i and b_i, c_i:

$$\pm\Delta(a_i - u_{\pm i}c_i) = u_{\pm i} - u_0 \tag{32}$$

and

$$\pm\Delta(b_i - v_{\pm i}c_i) = v_{\pm i} - v_0 \tag{33}$$

respectively. Provided that $u_i \neq u_{-i}$ or $v_i \neq v_{-i}$, which would mean that points $\boldsymbol{p}_i$ and $\boldsymbol{p}_{-i}$ do not lie on the same ray, equations (32) and (33) have unique solution

$$c_i = C_i/\Delta, \quad a_i = A_i/\Delta, \quad b_i = B_i/\Delta, \tag{34}$$

where

$$C_i = m_{-i} - m_i \tag{35}$$

and

$$A_i = m_{-i}u_i - m_i u_{-i}, \quad B_i = m_{-i}v_i - m_i v_{-i} \tag{36}$$

with

$$m_i = \frac{u_i - u_0}{u_i - u_{-i}} = \frac{v_i - v_0}{v_i - v_{-i}}, \quad m_{-i} = \frac{u_0 - u_{-i}}{u_i - u_{-i}} = \frac{v_0 - v_{-i}}{v_i - v_{-i}}. \tag{37}$$

Evidently expressions (14)-(15) and (23)-(24) can be rewritten in terms of A_i, B_i, C_i which means that parameters $D, \boldsymbol{\mathcal{P}}, \beta$ and γ can be determined without knowledge of value Δ. But, as it follows from (28), in order to determine the location of the focus in the scanner reference frame the value of Δ must be known.

5. Case $\beta = 0$

If the rotation axis is parallel to the detector plane, i.e. if $\beta = 0$, the values of all necessary system parameters can be obtained from projections of a single point acquired at different source positions, or equivalently, collected after successively rotating the point around the rotation axis.

To be more specific consider set $\{\boldsymbol{p}_k \in \mathbb{R}^3, k = 0, 1, 2, 3\}$ such that in the scanner reference frame $Oxyz$

$$\boldsymbol{p}_k = (\Delta \cos\alpha_k, \Delta \sin\alpha_k, z_0), \quad \alpha_k = \alpha_0 + k\pi/2, z_0 \neq 0. \tag{38}$$

So defined calibrating set is similar to the calibrating set considered in section 4 with the difference that it consists of four points only, located in the vertices of the square, which can be considered as vertices of the octahedron the vertical symmetry axis of which coincides with the rotation axis. In the following frame $Otsh$ axes Ot and Os of which are parallel to the diagonals of the square, and axis Oh coincides with the rotation axis, is considered as calibrating frame, and the center of the square, located in point $(0, 0, z_0)$, as initial point of the calibrating set. In spite of the fact that projections of four vertices only can be observed, nevertheless one can take advantage of the formalism developed in section 3. Let α_0 be the angle between the x-axis and the t-axis. Then the matrix of transformation from $Otsh$ to the detector reference frame $O\xi\eta\zeta$ is a matrix of two successive rotations, the rotation at an angle α_0 about h-axis and the rotation at an angle γ about the x-axis. That is,

$$\Theta = \begin{pmatrix} \cos\alpha_0 & \sin\alpha_0 & 0 \\ -\cos\gamma\sin\alpha_0 & \cos\gamma\cos\alpha_0 & \sin\gamma \\ \sin\gamma\sin\alpha_0 & -\sin\gamma\cos\alpha_0 & \cos\gamma \end{pmatrix} \tag{39}$$

According to (12), define vectors $\boldsymbol{c} = -\tau_0 D^{-1}\boldsymbol{\theta}_\xi, \boldsymbol{a} = \tau_0\boldsymbol{\theta}_\eta + \mathcal{P}_u\boldsymbol{c}, \boldsymbol{b} = \tau_0\boldsymbol{\theta}_\zeta + \mathcal{P}_v\boldsymbol{c}$, where $\boldsymbol{\theta}_\xi, \boldsymbol{\theta}_\eta$ and $\boldsymbol{\theta}_\zeta$ are the first, the second and the third row of matrix Θ respectively. Components c_i, a_i, b_i of these vectors can be derived for $i = t, s$ using approach described in section 4 (see (35)-(36)), and $c_h = 0$. Since $\|\boldsymbol{c}\| = \tau_0/D$ and for all $\gamma \in (-\pi/2, \pi/2)$

$$a_t c_s - a_s c_t = \frac{\tau_0^2}{D}\cos\gamma, \quad b_s c_t - b_t c_s = \frac{\tau_0^2}{D}\sin\gamma, \tag{40}$$

for missing coefficients a_h, b_h one obtains

$$a_h = \frac{b_s c_t - b_t c_s}{\|\boldsymbol{c}\|}, \quad b_h = \frac{a_t c_s - a_s c_t}{\|\boldsymbol{c}\|}. \tag{41}$$

Thus, if $\beta = 0$ the coefficients of the rational functions (11) can be determined from four projections of a point rotated successively at angle $\pi/2$ around the rotation axis. In order to use formulas derived in section 3 one has to set $c_h = 0$, $a_h^0 = a_h^1 = a_h$, $b_h^0 = b_h^1 = b_h$ and $\tau_1 = \tau_0$. Then formula (23) takes view

$$\tan\gamma = \frac{a_h}{b_h} = \frac{b_s c_t - b_t c_s}{a_t c_s - a_s c_t}, \tag{42}$$

while formulas (14)-(15) take view

$$D = \|\boldsymbol{c}\|^{-1}\sqrt{a_h^2 + b_h^2}, \quad (\mathcal{P}_u, \mathcal{P}_v) = (a_t c_t + a_s c_s, b_t c_t + b_s c_s)\|\boldsymbol{c}\|^{-2}, \tag{43}$$

Correspondingly, formulas (27),(28) become

$$z_0 = -V_0(a_h^2 + b_h^2)^{-1/2}, \quad (F_x, F_y) = (\|\boldsymbol{c}\|^{-1}, -U_0(a_h^2 + b_h^2)^{-1/2}), \tag{44}$$

where

$$\begin{pmatrix} U_0 \\ V_0 \end{pmatrix} = \begin{pmatrix} \cos\gamma & -\sin\gamma \\ \sin\gamma & \cos\gamma \end{pmatrix} \begin{pmatrix} u_0 - \mathcal{P}_u \\ v_0 - \mathcal{P}_v \end{pmatrix}. \tag{45}$$

If projections of $\boldsymbol{p}_k$ defined in (38) are not available the same formulas can be used after re-sampling that can be done as follows. The projection of circle $S := \{\boldsymbol{p}(\alpha) \in \mathbb{R}^3, \alpha \in [0, 2\pi)\}$ with $\boldsymbol{p}(\alpha) = (\Delta\cos(\alpha_0 + \alpha), \Delta\sin(\alpha_0 + \alpha), z_0)$ can be represented as

$$u(\alpha) = \frac{a_1\cos\alpha + a_2\sin\alpha + a_3}{1 + c_1\cos\alpha + c_2\sin\alpha}, \quad v(\alpha) = \frac{b_1\cos\alpha + b_2\sin\alpha + b_3}{1 + c_1\cos\alpha + c_2\sin\alpha}. \tag{46}$$

Unknown coefficients of the above functions can be recovered uniquely from five projections of $\boldsymbol{p}(\alpha) \in S$ acquired at $\alpha = 0$ and four other known values of α. Thereafter functions (46) can be evaluated analytically for any value of α, in particular for $\alpha_k = k\pi/2, k = 1, 2, 3$.

6. Influence of measurement errors

In section 3 it was shown that all system parameters can be expressed as functions of vectors $\boldsymbol{a}^k, \boldsymbol{b}^k, \boldsymbol{c}^k$, $k = 0, 1$, defined in (12). In turn, triple $(\boldsymbol{a}^k, \boldsymbol{b}^k, \boldsymbol{c}^k)$ is derived from the k-th projection of the calibrating set. Discrepancy from the presumably perfect calibrating set as well as measurement error cause the derived values to deviate from the values of interest. In this section expressions that relate the errors of important geometric parameters to deviations $\delta\boldsymbol{a}^k, \delta\boldsymbol{b}^k, \delta\boldsymbol{c}^k$ are presented. The bounds of these errors are obtained. Finally, dependence of deviations $\delta\boldsymbol{a}^k, \delta\boldsymbol{b}^k, \delta\boldsymbol{c}^k$ on measurement errors is studied, which should give an idea of how the geometry of the calibrating setup can influence the magnitude of errors.

Let $\delta a_i^k, \delta b_i^k, \delta c_i^k$, where $i = t, s, h$, be the components of the corresponding deviations in $Otsh$. Without loss of generality in this section the reference point of detector is assumed to be an orthogonal projection of the source. The following inequalities hold with high degree of accuracy (see appendix A):

$$L|\delta D|/D \le \chi_k\|\delta\boldsymbol{A}^k\| + \kappa_k\|\delta\boldsymbol{C}^k\|, \tag{47}$$

$$L|\delta\mathcal{P}_u|/D \le \chi_k\|\delta\boldsymbol{A}^k\| + \kappa_k\|\delta\boldsymbol{C}^k\|, \tag{48}$$

$$L|\delta\mathcal{P}_v|/D \le \chi_k\|\delta\boldsymbol{B}^k\| + \kappa_k\|\delta\boldsymbol{C}^k\|, \tag{49}$$

where Lf is a linear part of the Taylor expansion of f in powers of $\|\delta\boldsymbol{A}^k\|, \|\delta\boldsymbol{C}^k\|$, and

$$\chi_k = \frac{1}{\tau_k\Delta}, \quad \kappa_k = \frac{D}{\tau_k\Delta}. \tag{50}$$

Let $\lambda_k = \|\boldsymbol{C}^k\|\|\boldsymbol{C}^k + \delta\boldsymbol{C}^k\|^{-1}, k = 0, 1$, and let $\varepsilon = \lambda_0 - \lambda_1, \nu = \lambda_0 + \lambda_1$

For the errors of angles γ and β the following bounds are valid :

$$|\tan(\delta\gamma)| \le \frac{|\varepsilon|\alpha_{y,h} + \delta r}{2\alpha_{z,h}\cos\beta}, \quad |\tan(\delta\beta)| \le \frac{|\varepsilon|\alpha_{x,h} + \delta R}{\nu\alpha_{z,h}} \tag{51}$$

where $\alpha_{i,h}$ is cosine of the angle between axes $i \in \{x, y, z\}$ and h, and $\delta r, \delta R$ are small values such that $\delta r \to 0$ and $\delta R \to 0$ when $\max\{\|\delta\boldsymbol{A}^k\|, \|\delta\boldsymbol{B}^k\|, \|\delta\boldsymbol{C}^k\|\} \to 0$ (see appendix B). In particular, if $\beta = 0$, then $|\delta\gamma| \le \arcsin(\delta r_0)$, where $\delta r_0 = \tau_0^{-1}(\delta a_h^2 + \delta b_h^2)^{1/2}$ (see section 5 for definitions of a_h and b_h).

Since $|\varepsilon| \le \kappa_0\|\delta\boldsymbol{C}^0\| + \kappa_1\|\delta\boldsymbol{C}^1\|$, the bounds of both $\delta\mathcal{P}_u/D, \delta\mathcal{P}_v/D, \delta D/D$ and $\delta\gamma, \delta\beta$ are proportional to the magnitudes of $\chi_k\|\delta\boldsymbol{A}_k\|, \chi_k\|\delta\boldsymbol{B}_k\|$ and $\kappa_k\|\delta\boldsymbol{C}_k\|$. As it follows from (50), constants χ_k and κ_k depend on the size Δ of the calibrating set

and its location expressed by the scaling factor τ_k. Hence, they can be controlled. Norms $\|\delta \boldsymbol{A}^k\|, \|\delta \boldsymbol{B}^k\|$ and $\|\delta \boldsymbol{C}^k\|$, as well, depend not alone on the measurements errors but also on the size and location of the calibrating set in the scanner reference frame. One can find (see appendix C) that

$$\kappa_k \|\delta \boldsymbol{C}^k\| \leq \frac{4\sqrt{3}}{\tau_k} \frac{D}{\ell} \frac{\delta_m}{\Delta}, \tag{52}$$

$$\chi_k \|\delta \boldsymbol{A}^k\| \leq \frac{(2\rho_u + 1)\sqrt{3}}{\tau_k} \frac{\delta_m}{\Delta}, \tag{53}$$

$$\chi_k \|\delta \boldsymbol{B}^k\| \leq \frac{(2\rho_v + 1)\sqrt{3}}{\tau_k} \frac{\delta_m}{\Delta}, \tag{54}$$

where δ_m is a maximal absolute error of measurements, and

$$\ell = \min\{\max\{u_i - u_{-i}, v_i - v_{-i}\}, i \in \{t, s, h\}\}. \tag{55}$$

Values of ρ_u and ρ_v defined by

$$\rho_u = \frac{u_i + u_{-i} + \delta u_i + \delta u_{-i}}{u_i - u_{-i} + \delta u_i - \delta u_{-i}}, \tag{56}$$

$$\rho_v = \frac{v_i + v_{-i} + \delta v_i + \delta v_{-i}}{v_i - v_{-i} + \delta v_i - \delta v_{-i}}. \tag{57}$$

are very close to the values of fractions $(u_i + u_{-i})/(u_i - u_{-i})$ and $(v_i + v_{-i})/(v_i - v_{-i})$ respectively. Recall that in this section the orthogonal projection of the focus onto the detector is an origin of the detector. Therefore one can guarantee that, by fairly small misalignments and norm $\|\boldsymbol{p}_0\|$, $|\rho_u| \leq 1/2$ and $|\rho_v| \leq 1/2$.

7. Simulation and Results

We have simulated a situation in which the x-ray source and the detector are fixed in space and the calibrating set is put on the rotation table located between them. The setup used in the simulation was designed as follows. First, the scanner reference frame $Oxyz$ was defined as the one with the z-axis being rotation axis. The detector was assumed to be displaced from the ideal position in which the x-axis is perpendicular to the detector plane, intersects the detector in its center, and the rows of the detector are parallel to the y-axis. The displacement of the detector consists of two successive steps: 1) parallel carry in which the reference point of the detector is moved to location $\boldsymbol{R} = (R_x, R_y, R_z)$; 2) rotation at angles β and γ about the u-axis and the w-axis respectively, where the w-axis is normal to the detector. Finally the source focus was placed into location $\boldsymbol{F} = (F_x, F_y, 0)$. The true values of the focus to detector distance D and the components $\mathcal{P}_u, \mathcal{P}_v$ of the orthogonal projection of the focus can be calculated using (4).

Calibrating point was modeled as an apex of a conic body. We have preferred this approach to the conventional one, where a point is modeled as a ball's center, since this is easier to process numerically. Unlike an elliptical shadow of the ball, the shadow of a cone is the area bounded by two straight lines. The projection of the ball's center is generally neither in the center of its elliptical shadow nor in its focus. In order to identify it the gray value distribution within the ball's shadow must be analyzed. In contrast, localization of the projection of the cone apex comes down to detecting strong and clear boundaries of the cone's shadow. Detecting a boundary of the cone's shadow is done in two steps, 1) detecting edge

pixels $\{(u_p, v_p), p = 1, ..., N\}$ in the image I of the cone, and 2) constructing straight line $u\cos\phi + v\sin\phi = t$ that has the best fit to the set of detected edge pixels. Very accurate estimates of parameters ϕ, t are

$$\tan\phi_0 = \left(\sum_{p=1}^{N}(u_p - \overline{u})^2\right)^{1/2}\left(\sum_{p=1}^{N}(v_p - \overline{v})^2\right)^{-1/2}\mathrm{sgn}(\phi), \tag{58}$$

$$t_0 = \overline{u}\cos\phi^0 + \overline{v}\sin\phi^0, \tag{59}$$

where $\overline{u}, \overline{v}$ are mean values of sets $\{u_p\}$ and $\{v_p\}$ respectively. Additionally, in order to increase accuracy, edge profiles corresponding to different $\phi \in [\phi_0 - \delta\phi, \phi_0 + \delta\phi]$ with small $\delta\phi$ may be analyzed. The profile corresponding to a given ϕ is the function $g = g(s)$, where $s = u\cos\phi + v\sin\phi$ and $g(s) = I(u, v)$, that is, this is constituted by the grey values within the image region that contains the edge of the cone shadow. So, instead of ϕ_0 the value of ϕ may be chosen that corresponds to the steepest profile. At the same time one may replace value t^0 by value $t = \arg\max_s |g'_s(s)|$. For this paper, we settled for values ϕ_0, t_0 using (59) and (58) since these are nearly optimal. Nevertheless, the additional refinement described above could improve accuracy.

Hence, in order to identify the projection of the apex, both edges of the cone's shadow have to be detected as straight lines given by equations $u\cos\phi_i + v\sin\phi_i = t_i, i = 1, 2$. The projection of the cone apex is the solution of these equations.

The same cone was successively shifted into the predefined positions and its x-ray images were simulated each time using GEANT4 program. Thus, in order to get one complete projection of the calibrating set consisting of six points, as discussed in section 4, six images of the cone located in different positions have been simulated. Apparently, in the practice such an approach could be realized by means of a 3D translation stage. Then the axes of this stage would define calibrating frame $Otsh$. The simulated calibrating frame was defined as the one obtained from frame $Oxyz$ by means of two successive rotations at angles α_1 and α_2 about the h-axis and t-axis respectively.

The tables below show the true values of the considered geometric parameters used for the simulation and the residuum values which are the difference between the calculated value and the true value of parameter. The size of the detector's cell was set to 0.1 mm, and parameter $\Delta = 40$ mm.

TABLE 1. True values and residuum for parameters D, $\boldsymbol{\mathcal{P}}$ and $\boldsymbol{F}$

	D	$\mathcal{P}_u$	$\mathcal{P}_v$	F_x	F_y
True value (mm)	150.425	0.079	-13.198	101	1
Residuum (mm)	-0.003	0.016	0.106	0.013	7.0e-04

TABLE 2. True values and residuum for angles β and γ

	β	γ
True value	-5°	4°
Residuum	0.005°	0.008°

TABLE 3. True values and residuum for vector $\boldsymbol{R}$

	R_x	R_y	R_z
True value (mm)	-50	1	0
Residuum (mm)	0.003	0.004	0.113

In order to visually highlight the effect of the geometric calibration performed, we add two images: 1) reconstructed from the data generated for the case of misaligned geometry, and 2) reconstructed from the data one would collect after the scanner's adjustment appropriately to the values listed in the tables above.

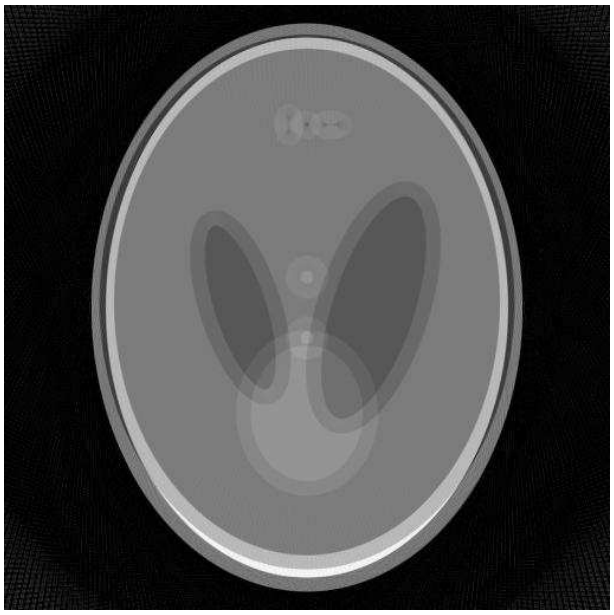

FIGURE 2. Central slice of the image reconstructed with FDK algorithm from the data of the Shepp-Logan phantom generated for the case of misaligned geometry.

8. Discussion and Conclusion

In this paper we have proposed a method of determining the geometry of a CT scanner designed for collecting cone-beam projections over circular source trajectory. The rotations axis of the scanner is assumed to be fixed. Therefore in the practice this method is suitable for the arrangement in which an object under study is rotated by means of a precision rotation stage placed between the source and the detector. For such a scanner it makes sense to consider the scanner reference frame $Oxyz$ which is constituted by rotation axis Oz and central plane Oxy. All expressions derived in the paper represent the desired geometrical parameters in this reference frame. Besides source to detector distance D, other parameters describing the geometry of the scanner are location $\boldsymbol{F}$ of the source, its orthogonal projection $\boldsymbol{\mathcal{P}}$ onto the detector, and position of the detector. There are different options to

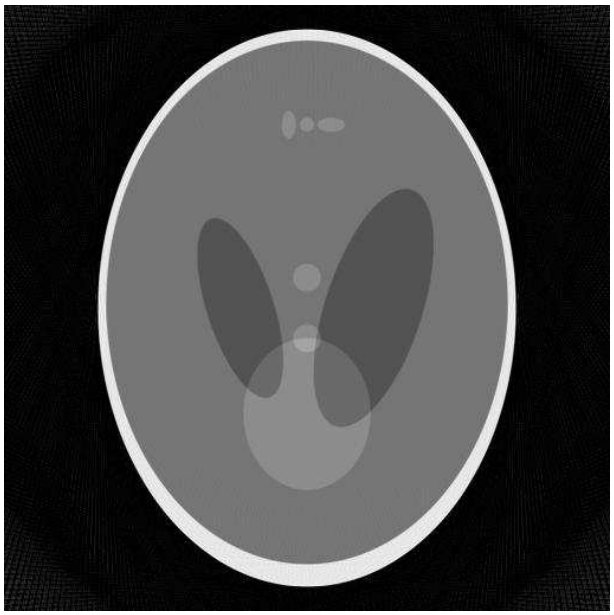

FIGURE 3. Central slice of the image reconstructed from the data one would collect after the scanner's adjustment appropriately to the values listed in the tables above.

direct axes x and y. In this paper the x-axis is directed perpendicularly to the line of intersection of the detector plane and the central plane (see Fig.3 in section 2). In such an arrangement the location of the source is described with two components F_x, F_y; the position of the detector is described with two Euler angles β and γ and three components of vector $\boldsymbol{R}$ pointing to the reference point of the detector . If the x-axis is directed to the source, the location of the source is described by the source to origin distance $\|\boldsymbol{F}\|$ only, while the orientation of the detector is described with three Euler angles α, β, γ. Both options are equivalent in terms of the number of degrees of freedom. Clearly, $\|\boldsymbol{F}\| = \sqrt{F_x^2 + F_y^2}$ and $\tan\alpha = F_y/F_x$.

The proposed method implies using calibrating phantom or in other words the set of calibrating points the relative positions of which are known in the orthogonal reference frame referred to in the paper as calibrating reference frame. This set can be treated as the set of sampling points of rational functions $u = u(\boldsymbol{p} - \boldsymbol{p}_0), v = v(\boldsymbol{p} - \boldsymbol{p}_0)$, where u, v are the observed components of the projection of point $\boldsymbol{p}$, and $\boldsymbol{p}_0$ is a point of the calibrating set called in the paper initial point. The unknown coefficients of these rational functions can be recovered uniquely from projections of the calibrating points (see section 3). Any calibrating set with sufficiently big number of points being in general position is suitable if the mutual arrangement of the points is known. Specifically in this paper the calibrating set consisting of six points located in the vertices of the octahedron was used. The center of the octahedron was considered as initial point $\boldsymbol{p}_0$ of the calibrating set. This set is preferable because of its simplicity both geometrically and in terms of simplicity of the math induced by this set. Also, the formalism developed for this set can be transferred directly to the situation where the detector is aligned with the rotation

axis, i.e. when $\beta = 0$. As studied in section 5, when $\beta = 0$, four projections of a single point rotated successfully at angle $\pi/2$ about the rotation axis are enough to solve the problem.

When none of geometric parameters is known, then two projections of a calibrating phantom are sufficient for the complete solution of the problem. If the scanner includes a shift of an object under study transversally to the central plane, then additionally the direction of the shift should be determined. As it was shown in the end of section 3 two more projections of the calibrating phantom are required to determine this direction.

In section 3 it was shown that parameter D, vectors $\boldsymbol{\mathcal{P}}$ and $\boldsymbol{F} - \boldsymbol{p}_0$, as well as matrix Θ expressing the transformation from the calibrating reference frame to the detector reference frame, can be determined from one projection of a calibrating phantom. It may be worth noting that these parameters provide full description of an individual *pose* of the scanner in the calibrating reference frame. Therefore the knowledge of these parameters is enough in applications where the source trajectory is uncertain, or such a concept as rotation axis does not make sense, or the magnitude of the so called flex of the rotation axis is substantial. Indeed, the only well defined reference frame, that is fixed in space, in such applications is the calibrating reference frame. The calibration of such scanning systems must be done individually for each cone-beam projection, or equivalently, for each individual pose of the scanner. In other words, each current pose of the scanner in the calibrating reference frame must be calculated during the patient scan.

In the focus of this paper there is a static micro CT scanner that has to be calibrated once or once over certain period of time. Under static micro CT scanner we mean a non-mobile device with a micro source focus and a high resolution large area detector, both fixed in space. It makes sense for such a scanner to know the geometrical parameter in the scanner reference frame, and the value of these parameters should be known as accurately as possible, ideally with accuracy specified by the resolution of the detector.

We have found that the error bounds of the calculated values is of the same order as δ/Δ, where δ is the measurement error, and Δ characterizes the size of the calibrating phantom. Namely, if ϵ is inaccuracy of the obtained value then $\epsilon \approx a\delta/\Delta$, where a is a constant that is inversely proportional to the scaling parameter τ_0, defined in Eq.13 on page 6, and proportional to the value of D/ℓ where ℓ characterizes the size of the projection of the phantom. As was shown in section 6, the magnitude of constant a also depends on location of the phantom in the scanner reference frame. Among all possible locations there are advantageous ones which are characterized both by small norm $\|\boldsymbol{p}_0\|$ and small distance between the initial point and line $\boldsymbol{F\mathcal{P}}$ connecting the focus and its orthogonal projection onto the detector plane. In section 6 there explicit expressions have been obtained that can be used for determining the magnitude of the inaccuracy depending on input error δ. Under assumption that the observation reference frame is orthogonal, parameter δ can be considered as a sum of measurement error and the error caused by imperfectness of the calibrating phantom.

The method is assumed to be used for estimating geometric parameters of static micro CT scanner with circular source trajectory. Since small inaccuracies in ray coordination can lead to artefacts, noticable in reconstructed images on the corresponding scale, the geometry of such a scanner must be known with accuracy

specified by the resolution of its detector. The study shows that appropriately arranging the calibrating setup the proposed method can be a practical tool for accomplishing this task.

Appendix A

If the reference point of detector is an orthogonal projection of the source, then $\mathcal{P}_u = \mathcal{P}_v = 0$, and vectors $\boldsymbol{a}^k, \boldsymbol{b}^k, \boldsymbol{c}^k$, where $k \in \{0, 1\}$, are mutually orthogonal. From (14) it follows that

$$D + \delta D = \frac{\|(\boldsymbol{a}^k + \delta\boldsymbol{a}^k) \times (\boldsymbol{c}^k + \delta\boldsymbol{c}^k)\|}{\|\boldsymbol{c}^k + \delta\boldsymbol{c}^k\|^2}. \tag{60}$$

Under assumption that $\delta\boldsymbol{c}^k$ and $\delta\boldsymbol{a}^k$ are independent from each other, inequality

$$\frac{\|\boldsymbol{a}^k\| - \|\delta\boldsymbol{a}^k\|}{\|\boldsymbol{c}^k\| + \|\delta\boldsymbol{c}^k\|} \le D + \delta D \le \frac{\|\boldsymbol{a}^k\| + \|\delta\boldsymbol{a}^k\|}{\|\boldsymbol{c}^k\| - \|\delta\boldsymbol{c}^k\|} \tag{61}$$

defines the range of values $D + \Delta D$ for constant $\|\delta\boldsymbol{c}^k\|$ and $\|\delta\boldsymbol{a}^k\|$. After recalling that $\boldsymbol{a}^k = \boldsymbol{A}^k/\Delta$ (see (36) for definition of $\boldsymbol{A}^k$) and noting that $D = \|\boldsymbol{a}^k\|/\|\boldsymbol{c}^k\|$ last inequality can be rewritten in form

$$\frac{|\delta D|}{D} \le \frac{\chi_k\|\delta\boldsymbol{A}^k\| + \kappa_k\|\delta\boldsymbol{C}^k\|}{1 - \kappa_k\|\delta\boldsymbol{C}^k\|}, \tag{62}$$

Expanding the right part of the last expression in powers of $\|\delta\boldsymbol{A}^k\|, \|\delta\boldsymbol{C}^k\|$ and leaving only linear terms yields (47). From (15) it follows that

$$\delta\mathcal{P}_u = \frac{\langle\boldsymbol{a}^k, \delta\boldsymbol{c}^k\rangle + \langle\delta\boldsymbol{a}^k, \boldsymbol{c}^k + \delta\boldsymbol{c}^k\rangle}{\|\boldsymbol{c}^k + \delta\boldsymbol{c}^k\|^2}, \tag{63}$$

Expanding the right part of this expression in powers of $\|\delta\boldsymbol{A}^k\|, \|\delta\boldsymbol{C}^k\|$ and leaving linear terms one obtains inequalitiy (48). Similarly one obtains inequality (49).

Appendix B

In order to find an error $\delta\gamma$ rewrite (21) in form

$$\tan(\gamma + \delta\gamma) = \frac{\omega_{\eta,h} + \delta\omega_{\eta,h}}{\omega_{\zeta,h} + \delta\omega_{\zeta,h}}. \tag{64}$$

One can find that

$$\omega_{i,h} + \delta\omega_{i,h} = D(\lambda_0\theta^0_{i,h} + \lambda_1\theta^1_{i,h} + \delta\omega_i), \quad i = \eta, \zeta \tag{65}$$

with $\lambda_k = \|\boldsymbol{c}^k + \delta\boldsymbol{c}^k\|^{-1}\|\boldsymbol{c}^k\|$, and

$$\begin{pmatrix}\delta\omega_\eta \\ \delta\omega_\zeta\end{pmatrix} = \frac{1}{\Delta}\sum_{k=0}^{1}\frac{\lambda_k}{\tau_k}\begin{pmatrix}\delta A^k_h - (C^k_h + \delta C^k_h)\delta\mathcal{P}_u \\ \delta B^k_h - (C^k_h + \delta C^k_h)\delta\mathcal{P}_v\end{pmatrix} \tag{66}$$

Recalling that $(\theta^k_{\xi,h}, \theta^k_{\eta,h}, \theta^k_{\zeta,h})^T$ is the third column of matrix $\Theta^k = \mathcal{GBA}^k$, and substituting equations (21) and (64) into formula

$$\tan(\delta\gamma) = \frac{\tan(\gamma + \delta\gamma) - \tan\gamma}{1 + \tan(\gamma + \delta\gamma)\tan\gamma} \tag{67}$$

yields

$$\tan(\delta\gamma) = \frac{\varepsilon\alpha_{y,h} + \delta\omega_\eta\cos\gamma - \delta\omega_\zeta\sin\gamma}{\nu_1 + \delta\omega_\eta\sin\gamma + \delta\omega_\zeta\cos\gamma}, \tag{68}$$

where we have introduced values

$$\varepsilon = \lambda_0 - \lambda_1, \quad \nu = \lambda_0 + \lambda_1, \quad \nu_1 = \nu\alpha_{z,h}\cos\beta + \varepsilon\alpha_{x,h}\sin\beta. \tag{69}$$

To obtain the bounds of $\delta\gamma$ rewrite (68) in form

$$\tan(\delta\gamma) = \frac{\varepsilon\alpha_{y,h} + \delta r\cos(\varphi+\gamma)}{\nu_1 + \delta r\sin(\varphi+\gamma)}, \tag{70}$$

where $\tan\varphi = \delta\omega_\zeta/\delta\omega_\eta$, $\delta r = (\delta\omega_\eta^2 + \delta\omega_\zeta^2)^{1/2}$, and find extrema of the expression on the right hand side of (70) regarded as a function of φ. One can check that with accuracy up to the linear terms of the expansion in powers of ε and δr

$$\max_\varphi |\tan(\delta\gamma)| \approx \frac{|\varepsilon|\alpha_{y,h} + \delta r}{2\alpha_{z,h}\cos\beta}, \tag{71}$$

In the special case, considered in section 5, one has to set $\lambda_0 = \lambda_1$, $\alpha_{z,h} = 1$. Then (70) takes view

$$\tan(\delta\gamma) = \frac{\delta r_0\sin(\varphi_0-\gamma)}{1+\delta r_0\cos(\varphi_0-\gamma)}, \tag{72}$$

with $\tan\varphi_0 = \delta a_h/\delta b_h$ and $\delta r_0 = \tau_0^{-1}(\delta a_h^2 + \delta b_h^2)^{1/2}$. In this case $\max_{\varphi_0}|\tan(\delta\gamma)| = \tan\arcsin(\delta r_0)$. Therefore

$$|\delta\gamma| \le \arcsin(\delta r_0). \tag{73}$$

In order to estimate error $\delta\beta$ rewrite (22) in form $\tan\beta = -\omega_{\xi,h}D(\omega_{\eta,h}^2 + \omega_{\zeta,h}^2)^{-1/2}$. Then

$$\tan(\beta+\delta\beta) = -\frac{(\omega_{\xi,h}+\delta\omega_{\xi,h})(D+\delta D)}{\sqrt{(\omega_{\eta,h}+\delta\omega_{\eta,h})^2 + (\omega_{\zeta,h}+\delta\omega_{\zeta,h})^2}}. \tag{74}$$

Values $\omega_{\eta,h}+\delta\omega_{\eta,h}$ and $\omega_{\zeta,h}+\delta\omega_{\zeta,h}$ are defined in (65) and (66), and

$$\omega_{\xi,h} + \delta\omega_{\xi,h} = \lambda_0\theta^0_{\xi,h} + \lambda_1\theta^1_{\xi,h} - D\delta\omega_\xi, \tag{75}$$

where $\delta\omega_\xi = \lambda_0\tau_0^{-1}\delta c_h^0 + \lambda_1\tau_1^{-1}\delta c_h^1$. One can check that

$$\tan(\beta+\delta\beta) = \frac{-\nu_2 + D\delta\omega_\xi}{\nu_1 + \delta\omega_\eta\sin\gamma + \delta\omega_\zeta\cos\gamma}\mu \tag{76}$$

where $\nu_2 = -\nu\alpha_{z,h}\sin\beta + \varepsilon\alpha_{x,h}\cos\beta$ and $\mu = (1 + D^{-1}\delta D)\cos(\delta\gamma)$. Applying formula similar to (67) yields

$$\tan(\delta\beta) = \frac{-\varepsilon\alpha_{x,h} + \varepsilon_1\cos\beta - (\delta\omega_\eta\sin\gamma + \delta\omega_\zeta\cos\gamma)\sin\beta}{\nu\alpha_{z,h} + \varepsilon_1\sin\beta + (\delta\omega_\eta\sin\gamma + \delta\omega_\zeta\cos\gamma)\cos\beta} \tag{77}$$

with $\varepsilon_1 = (1-\mu)\nu_2 + \mu D\delta\omega_\xi$. The bounds of error $\delta\beta$ can be obtained in a way similar to that used for obtaining the bounds of $\delta\gamma$, i.e. one rewrites (77) in form

$$\tan(\delta\beta) = \frac{-\varepsilon\alpha_{x,h} + \delta R\sin(\vartheta-\beta)}{\nu\alpha_{z,h} + \delta R\cos(\vartheta-\beta)} \tag{78}$$

where

$$\tan\vartheta = \frac{\mu D\delta\omega_\xi + \nu_1(1-\mu)}{\delta\omega_\eta\sin\gamma + \delta\omega_\zeta\cos\gamma}, \tag{79}$$

$$\delta R = \sqrt{(\mu D\delta\omega_\xi + \nu_1(1-\mu))^2 + (\delta\omega_\eta\sin\gamma + \delta\omega_\zeta\cos\gamma)^2}, \tag{80}$$

and finds the extrema of the expression on the right hand side of (78) considered as function of ϑ. One can check that approximation

$$\max_{\vartheta} |\tan(\delta\beta)| \approx \frac{|\varepsilon|\alpha_{x,h} + \delta R}{\nu\alpha_{z,h}} \left(1 - \frac{|\varepsilon|\alpha_{x,h}}{\nu\alpha_{z,h}} \frac{\delta R}{\nu\alpha_{z,h}}\right)^{-1} \tag{81}$$

is valid with accuracy up to the second order terms of the expansion in powers of small values ε/ν and $\delta R/\nu$.

Appendix C

Assume that the calibrating set considered in section 4 has been used for the determination of coefficients $\boldsymbol{a}, \boldsymbol{b}, \boldsymbol{c}$, where superscripts 0 and 1 have been omitted for simplicity of notations. Using (35)-(36) one obtains

$$\delta C_i = \delta m_{-i} - \delta m_i, \tag{82}$$

$$\delta A_i = (m_{-i} + \delta m_{-i})(u_i + \delta u_i) - (m_i + \delta m_i)(u_{-i} + \delta u_{-i}) - A_i, \tag{83}$$

$$\delta B_i = (m_{-i} + \delta m_{-i})(v_i + \delta v_i) - (m_i + \delta m_i)(v_{-i} + \delta v_{-i}) - B_i \tag{84}$$

where $i \in \{t, s, h\}$, and δm_i can be estimated either with the help of formula

$$\delta m_i = \frac{m_{-i}\delta u_i + m_i\delta u_{-i} - \delta u_0}{u_i - u_{-i} + \delta u_i - \delta u_{-i}} \tag{85}$$

or

$$\delta m_i = \frac{m_{-i}\delta v_i + m_i\delta v_{-i} - \delta v_0}{v_i - v_{-i} + \delta v_i - \delta v_{-i}} \tag{86}$$

depending on which option is selected for the calculation of coefficient m_i (see (37)). Let $u_i \geq u_{-i}$ and $v_i \geq v_{-i}$. Then under assumption that calibrating points $\boldsymbol{p}_i, \boldsymbol{p}_{-i}$ do not lie on the same ray, both m_i and m_{-i} are positive, and

$$m_i + m_{-i} = 1. \tag{87}$$

Provided that option (85) is selected

$$|\delta m_i| \leq \frac{|m_{-i}\delta u_i + m_i\delta u_{-i}| + |\delta u_0|}{u_i - u_{-i} + \delta u_i - \delta u_{-i}}. \tag{88}$$

Therefore

$$|\delta m_i| \leq \frac{2\delta_m}{\ell - 2\delta_m} \tag{89}$$

where δ_m is the maximal absolute error of measurements, and

$$\ell = \min\{\max\{u_i - u_{-i}, v_i - v_{-i}\}, i \in \{t, s, h\}\}. \tag{90}$$

It can be checked that

$$\delta m_{-i} = -\delta m_i. \tag{91}$$

Therefore

$$|\delta C_i| = 2|\delta m_i| \tag{92}$$

(see (82)). Accounting for equation (88), one obtains inequality

$$|\delta C_i| \leq 4\delta_m/\ell \tag{93}$$

that holds with high accuracy when value δ_m/ℓ is small.

In order to estimate the bounds of error $\delta\boldsymbol{A}$ rewrite (83) in form

$$\delta A_i = (u_i + u_{-i} + \delta u_i + \delta u_{-i})\delta m_{-i} + m_{-i}\delta u_i - m_i\delta u_{-i}, \tag{94}$$

where equality (91) has been taken into account. Therefore for absolute value of δA_i inequality

$$|\delta A_i| \le |u_i + u_{-i} + \delta u_i + \delta u_{-i}||\delta m_i| + m_{-i}|\delta u_i| + m_i|\delta u_{-i}| \le \\ \le |u_i + u_{-i} + \delta u_i + \delta u_{-i}||\delta m_i| + \delta_m \le (2\rho_u + 1)\delta_m \tag{95}$$

is valid, where

$$\rho_u = \frac{u_i + u_{-i} + \delta u_i + \delta u_{-i}}{u_i - u_{-i} + \delta u_i - \delta u_{-i}}. \tag{96}$$

The same considerations are valid also for discrepancy δB_i. Hence, for the norms $\|\delta \boldsymbol{A}\|, \|\delta \boldsymbol{B}\|$ one obtains bounds

$$\|\delta \boldsymbol{A}\| \le (2\rho_u + 1)\sqrt{3}\delta_m, \quad \|\delta \boldsymbol{B}\| \le (2\rho_v + 1)\sqrt{3}\delta_m. \tag{97}$$

Therefore

$$\chi_k \|\delta \boldsymbol{A}^k\| \le \frac{(2\rho_u + 1)\sqrt{3}}{\tau_k}\frac{\delta_m}{\Delta}, \quad \chi_k \|\delta \boldsymbol{B}^k\| \le \frac{(2\rho_v + 1)\sqrt{3}}{\tau_k}\frac{\delta_m}{\Delta} \tag{98}$$

The norm $\|\delta \boldsymbol{C}\|$ is bounded by

$$\|\delta \boldsymbol{C}\| \le 4\sqrt{3}\delta_m/\ell. \tag{99}$$

Correspondingly

$$\kappa_k \|\delta \boldsymbol{C}^k\| \le \frac{4\sqrt{3}}{\tau_k}\frac{D}{\ell}\frac{\delta_m}{\Delta}. \tag{100}$$

References

[1] D. Béqué, J. Nuyts, G. Bormans, P. Suetens and P. Dupont, "Characterization of pinhole SPECT acquisition geometry," in *IEEE Transactions on Medical Imaging*, **22**, (5), (2003), 599-612, doi: 10.1109/TMI.2003.812258

[2] A V Bronnikov, Virtual alignment of x-ray cone-beam tomography system using two calibration aperture measurements, *Optical Engineering* 38 (1999): 381–386.

[3] A V Bronnikov, A new algorithm for geometric self-calibration in cone-beam CT, *Proc. 11th Int. Meeting on Fully 3D Image Reconstruction in Radiology and Nuclear Medicine*, (2011) pp 175–8

[4] Cho Y, Moseley DJ, Siewerdsen JH, Jaffray DA. Accurate technique for complete geometric calibration of cone-beam computed tomography systems, *Med. Phys* **32**, 2005, 968-983

[5] M. Defrise, C. Vanhove and J. Nuyts, "Perturbative Refinement of the Geometric Calibration in Pinhole SPECT," *IEEE Transactions on Medical Imaging*, **27**, (2) , (2008), 204-214, doi: 10.1109/TMI.2007.904687

[6] Ford JC, Zheng DD, Williamson JF Estimation of CT cone-beam geometry using a novel method insensitive to phantom fabrication inaccuracy: Implications for isocenter localization accuracy, Medical Physics 38 (2011), 2829–2840.

[7] G. T. Gullberg, B. M. W. Tsui, C. R. Crawford, and E. R. Edgerton, Estimation of geometrical parameters for fan beam tomography, *Phys. Med. Biol.*, **32**, (12), (1987), 1581-1594.

[8] Gullberg G, Tsui B, Crawford C, Ballard J and Hagius J, Estimation of geometrical parameters and collimator evaluation for cone-beam tomography, *Med. Phys.*, **17**, (1990), 264-272

[9] Matthew W. Jacobson and Michael D. Ketcha and S Capostagno and Alberto Martín and Ali Uneri and Joseph Görres and Tharindu De Silva and Sureerat Reaungamornrat and Renmin Han and Amir Manbachi and J. Webster Stayman and Sebastian Vogt and Gerhard Kleinszig and Jeffrey H. Siewerdsen, A line fiducial method for geometric calibration of cone-beam CT systems with diverse scan trajectories. *Phys. Med. Biol.*, **63** 2, (2018) 025030

[10] Khoury R, Bonissent A, Clémens JC, Meessen C, Vigeolas E, et al. A geometrical calibration method for the PIXSCAN micro-CT scanner, *Journal of Instrumentation* 4, (2009), 07016

[11] Kyriakou Y, Lapp R M, Hillebrand L, Ertel D and Kalender W A 2008 Simultaneous misalignment correction for approximate circular conebeam computed tomography, *Phys. Med. Biol.*, 53 6267–89

[12] Catherine Mennessier, Rolf Clackdoyle, Frederic Noo, Direct determination of geometric alignment parameters for cone-beam scanner, *Physics in Medicine and Biology*, **54**, (2009), 1633-1660.

[13] Frederic Noo, Rolf Clackdoyle, Catherine Mennessier, Timothy A White and Timothy J Roney, Analytic method based on identification of ellipse parameters for scanner calibration in cone-beam tomography, *Physics in Medicine and Biology*, **45**(11), (2000),3489-3508.

[14] Ouadah S, Stayman J W, Gang G J, Ehtiati T and Siewerdsen J H, Self-calibration of cone-beam CT geometry using 3D–2D image registration, *Phys. Med. Biol.*, **61**, (2016), 2613–32

[15] Panetta D, Belcari N, Del Guerra A, Moehrs S, An optimization-based method for geometrical calibration in cone-beam CT without dedicated phantoms. *Phys. Med. Biol.*, **53**, (2008), 3841–3861

[16] Patel V, Chityala R N, Hoffmann K R, Ionita C N, Bednarek D R and Rudin S Self-calibration of a cone-beam micro-CT system, *Med. Phys.*, **36**, (2009), 48–58

[17] Rougee A, Picard C, Ponchut C, Trousset Y Geometrical calibration of x-ray imaging chains for three-dimensional reconstruction, *Computerized Medical Imaging and Graphics the Official Journal of the Computerized Medical Imaging Society* 17: 295, (1993)

[18] Robert N, Watt KN, Wang XY, Mainprize JG The geometric calibration of cone-beam systems with arbitrary geometry, *Physics in Medicine and Biology* 54, (2009) , 7239–7261.

[19] von Smekal L, Kachelriess M, Stepina E, Kalender W.A. Geometric misalignment and calibration in cone-beam tomography, *Medical Physics*, **21**(12), (2004), 3242-3266.

[20] Wicklein J, Kunze H, Kalender W A and Kyriakou Y Image features for misalignment correction in medical flat-detector CT, *Med. Phys.*, **39**, (2012), 4918

[21] Yang K, Kwan A L C, Miller D F and Boone, A geometric calibration method for cone beam CT systems, *Med. Phys.*, 33 (2006), 1695–706

[22] Yan, B., Zhang, F., Du, J.P., Iterative geometric calibration in circular cone-beam computed tomography, *Optik*, **125**, (11), (2014), 2509-2514.

[1] Helmholtz Zentrum Muenchen, D-85764 Neuherberg, Germany
Email address: oleg.tischenko@helmholtz-muenchen.de

[2] Otto-von-Guericke University, Magdeburg, Germany
Email address: nazila.saeid@ovgu.de
Email address: christoph.hoeschen@ovgu.de